Indian Journal of Science and Technology, Vol 9(36), DOI: 10.17485/ijst/2016/v9i36/96985, September 2016
ISSN (Print) : 0974-6846
ISSN (Online) : 0974-5645

Performance Analysis, Modeling and Control of Multi-Port DC-DC Boost Converter for an Integrated Power Generation System

V. Indragandhi[1*] and A. Benitto[2]

[1]School of Electrical Engineering, VIT University, Vellore - 632014, Tamil Nadu, India; arunindra08@gmail.com
[2]Thiagarajar College of Engineering, Madurai - 625015, Tamil Nadu, India; benitto3@gmail.com

Abstract

Objective: This paper presents a new DC-DC boost converter for renewable hybrid power generation scheme is designed using five controllable switches in its unified structure. **Methods/ Statistical Analysis:** In this research work, converter operation is discussed with four different operating modes based on the renewable resources availability. To rectify the difficulties associated with controller design of this converter, multi input - multi output controller design is obtained by deducing the small signal equations and state space modeling for all the operating modes. In this study, MATLAB/Simulink is used to design the model for DC-DC boost converter. A strategy to manage the power flow between the different energy sources is presented. **Findings:** Uncomplicated structure, centralized control, transformer-less operation, less weight, highly stable and increased output voltage is the best qualities of the designed converter. This study demonstrates that the overall power management is efficient and demand is balanced successfully. **Applications/Improvement:** This research helps to find the best power electronic converter structure for renewable based hybrid power generation system.

Keywords: DC-DC Converter, Dynamic Modeling, Hybrid Systems, Power Management, Renewable Energy

1. Introduction

Three port converters are found to be better than conventional system which uses multiple converters. Because of its advantages such as superior system efficiency, faster response, fewer components, compact packaging and unified power management[1–3]. A dual active bridge topology is found to be commonly popular among the bi-directional DC-DC converters[4–6] that uses two half bridges or two full bridges in the high frequency transformer that has phase shift control ensuing in zero voltage switching and flexible power flow control.

A high efficiency Zero Voltage Switching (ZVS) multi-input converter directly utilized the current-source type applying for both input power sources[7]. This method offers a reduction in conduction loss of switches in the dual-power-supply state depending on the designed Pulse Width Modulation (PWM) signals and series-connected input circuits. In order to achieve turn-on ZVS of the switches, an auxiliary circuit with a small inductor functioning in the Discontinuous Conduction Mode (DCM) was used[8]. It is possible to remove the huge reverse-recovery current of the output diode through auxiliary inductor which is connected to Schottky diode[8].

An interleaved method that can alleviate the output voltage ripple of the two-input inductor currents is proposed in[9]. Thus, this converter was beneficial to convert two power sources of different voltages to a single DC-bus voltage. This converter can be used both in single as well as dual power supply states. A two-input power converter that has a ZVS for hybrid Fuel Cell and battery power system[10]. However, this converter could neither deliver a bi-directional functionality nor could boost the input voltage, despite having well developed circuit efficiency.

In[11] a novel three-input DC-DC boost converter that could be used for hybrid power system applications. The proposed method was able to produce current-source type in the input power ports that could control the input voltages.

*Author for correspondence

This method was successfully used to control the power flow between the input sources and the load, using duty ratios. In[12] a three-input DC-DC converter for grid-connected hybrid power system fed from full bridge inverter with a bi-directional flow is presented. In this model, the presence of transistors resulted in Total Harmonic Distortion (THD) and switching losses and the four-port DC-DC converter is also introduced with decoupling and small signal modeling. In this work, soft switching multi-port DC-DC boost converter designed for hybrid power generation.

In[13] a novel multi-input bidirectional DC-DC boost converter which connects a Fuel Cell, storage and load with a mixture of a DC linkage and magnetic-coupling is presented. A boost-two half-bridge and a bidirectional direct-connected switching cells are utilized. The topology is uncomplicated and requires only minimum number of power switching devices. A converter to fulfill the energy needs of many modern systems that harvesting from numerous sources and the supervision of power storage is proposed in[14,15]. The implementation of the converter a scheme is purposely modified for such applications and suggests this great development potential over conventional methods. In[16,17] a new isolated current-fed DC-DC converter with two input power sources based on multi-transformer is designed, which is appropriate for Fuel Cells and super-capacitors hybrid system. The design and analysis of a satellite power system, which makes use of three-port converters to interface a range of autonomous solar panel, one battery to a regulated bus is presented in[17,18]. The features of the converter are minimum component and compact configuration. The interleaved three port converters boost the power and offer redundancy.

Recently, multi-input converters offer a promising solution for the replacement of many power conversion steps over the conventional hybrid system, which joins various renewable sources in its single structure[19–21]. These converters have acknowledged more concentration in the literature due to its uncomplicated circuit, bi-directional power flow with storage, good reliability, minimum manufacturing cost and compact size[22]. Considering the above advantages, a new circuit topology for multi-port converter is proposed in this research. The paper is presented as follows. Section 2 shows the proposed converter structure. Section 3 explains the operating principles of the proposed system. Section 4 presents the experimental results of all the stages. Section 5 deals with modeling and performance evaluation of proposed system and Section 6 concludes the research work.

2. Proposed Method of Hybrid Power Generation

In this research study, a DC-DC boost converter that uses the wind, Photo voltaic (PV), Fuel Cell (FC) and battery input sources for hybrid power generation system is proposed[22]. The proposed converter with unified structure consists of three unidirectional input ports, which act as input power sources; a bi-directional input port for storage and an output load port as shown in Figure 1. PV and FC input ports function as constant current-source type as well as build up the input voltages. This is a unique arrangement availing just five power MOSFET switches; each of the switches uses different duty ratios and hence controlled individually. The duty ratios also control the power flow between the input sources. The excess power generated through the PV and FC is directed to the battery for storage. Depending on the energy utilization by the storage element, four different power operation modes of the converter are defined.

The proposed method have significant advantages over the conventional method of PV, FC, wind and battery input sources which have a separate conversion system .The proposed converter uses fewer inductors and switches, low-voltage batteries, produces high voltage and it functions in highly stable operating conditions. Further, the power generated by the input sources is distributed both to the load and the battery individually or simultaneously. Due to an independent control of duty ratios of the switches, the restriction in the summing up of the duty ratios is eradicated resulting in a high output voltage. The advantages are the proposed converter can be used as a powerful substitute for the multiple source wind, PV and FC hybrid power systems. Further, a few

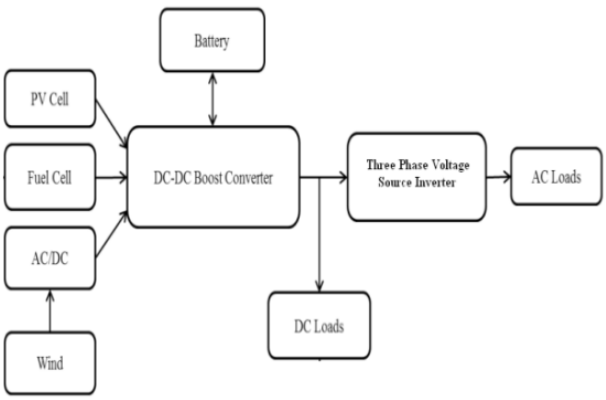

Figure 1. Block diagram of the proposed converter.

advantages are enumerated as follows: Uncomplicated structure, centralized control, transformer-less operation, less weight, highly stable and increased output voltage. Various functions such as attaining maximum power point operation of the PV source, adjusting the power setting in the FC, battery charging and discharging and controlling the output voltage are addressed by controlling the switches duty ratio.

3. Multi-Port Converter Operation

For effective working of the input sources, the following conditions should be satisfied: The switch S2 and S3 should not be turned off before S1 is switched off; else L2 and L3 will continue to store energy even if S1 is switched off, which will be an undesirable outcome. To ensure that S1 remains off before starting S2 and S3, the following inequality should be completed for the converter: Duty ratios 2 and 3 should be greater than duty ratio 1, similar to the conventional type boost converters, diodes D1 and D2 conducts with corresponding switches S1, S2 and S3 in a complementary mode as shown in Figure 2.

Multi-port boost converter is addressed through four different modes of operation and for each mode of operation state space model equations are derived. During one switching period a minimum of two sources should be used to generate the required power. Total power demand met by all the input sources is given by:

$$P_{load} = P_{FC} + P_{wind} + P_{PV} + P_{bat} \quad (1)$$

3.1 Mode-1 Operation

In the first mode, power is supplied to the load by wind and PV cell, without FC and battery. At this point, switches S1, S2 and S3 are turned ON. The duty ratio of switch S1 should be less than that of S2 and S3. Turning ON of all the switches consequently charges the inductors L1 and L2. Switching OFF of the three switches, results in the discharging of inductors through the diodes D1 and D2 to the load. Figure 3 illustrates the circuit for Mode 1 operation and Figure 4 depicts the key waveforms of gate signal and inductor current. The charging of an inductor L1 is performed until turning off the switch S1 and it is discharged with voltage Vw-V0 into the load. Similarly, the inductor L2 is charged until turning off the switch S2 and S3 and it is discharged with voltage VPV -V0 into load. The switch S1 is turned off before the switches S2 and S3. Small signal modeling of the mode-1 operation is derived as follows:

$$L_1 \frac{di_{L1}}{dt} = d_1 V_W + (1 - d_1)(V_W - V_0) \quad (2)$$

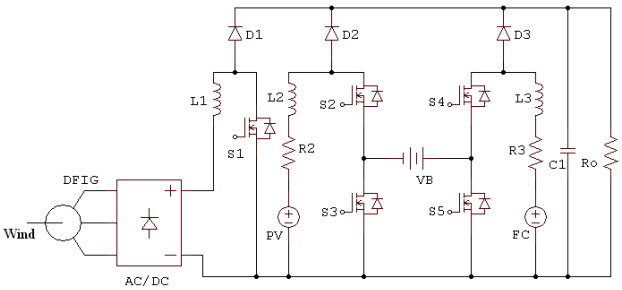

Figure 2. Proposed DC-DC boost converter topology.

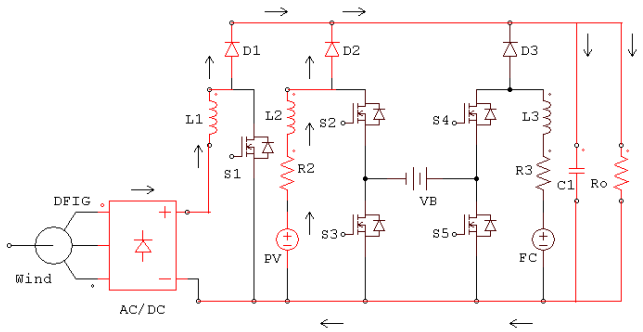

Figure 3. Circuit for operating mode-1.

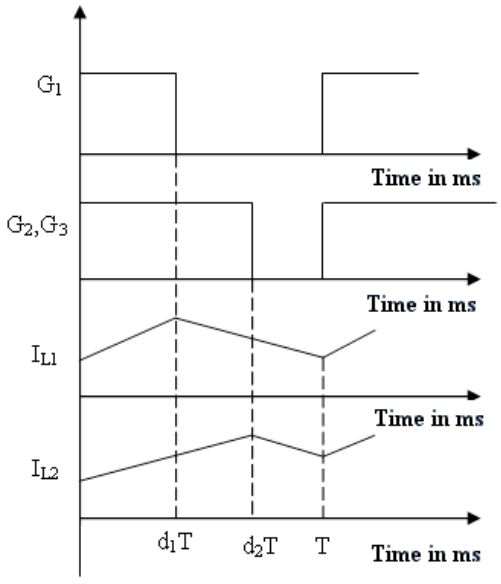

Figure 4. Key waveforms for mode-1 operation.

$$\frac{V_W - L_1\frac{di_{L1}}{dt}}{1-d_1} = V_0 \quad (3)$$

$$L_2\frac{di_{L2}}{dt} + r_2 i_{L2} = d_2 V_{PV} + (1-d_2)(V_{PV} - V_0) \quad (4)$$

$$\frac{V_{PV} - L_2\frac{di_{L2}}{dt} - r_2 i_{L2}}{1-d_2} = V_0 \quad (5)$$

$$C_1\frac{dV_0}{dt} + \frac{V_0}{R_0} = i_{L1} + i_{L2} - d_1 i_{L1} - d_2 i_{L2} \quad (6)$$

$$\text{If } P_{load} \leq P_{wind} + P_{PV}, \quad (7)$$

Then the converter stabilizes the DC voltage by wind and PV energy, whereas FC and battery are kept on standby. Where *P* load = load demand; *P* wind = power generated by the wind turbines:

*P*PV = power generated by PV system.

$$P_{FC} = P_{bat} = 0 \quad (8)$$

$$P_{load} = P_{wind} + P_{PV} \quad (9)$$

The maximum power point tracking of the PV and wind is achieved through the DC–DC boost converter, thus regulating the DC load voltage, where $P_{load} > P_{wind} + P_{PV}$ (10).

3.2 Mode-2 Operation

Another mode is also attempted to achieve the load demand when wind is poor, here the load receives power supply from PV, FC and discharging of the battery. The switches S2, S4 and S5 are turned ON resulting in the charging of the inductors L2 and L3. In the beginning, the switch S4 is turned OFF to enable the battery discharging mode with extra power, followed by turning OFF of the switches S2 and S5. The current flows through the diodes D2 and D3 by discharging the energy stored in the inductors L2 and L3. Figure 5 shows the circuit for this mode of operation and the key waveforms of gate signal and inductor current are shown in Figure 6. In this mode, the duty cycle of switches are fixed such that the battery discharging should not cross beyond its maximum limit. The inductor L2 is charged with VPV+ VB. The inductors L2 and L3 are discharged with voltages VPV-V0 and VFC-V0 respectively. Small signal modeling of the mode-2 operation is derived as follows:

$$P_{load} = P_{FC} + P_{BAT} + P_{PV} \quad (11)$$

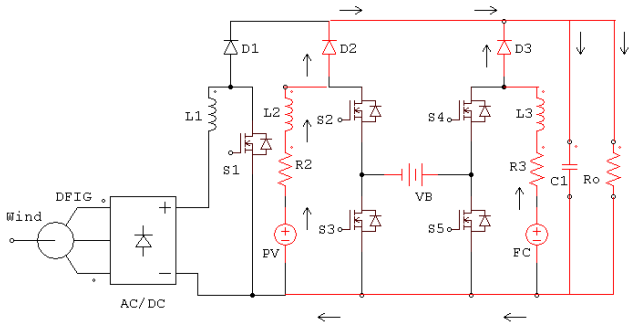

Figure 5. Circuit for operating mode-2.

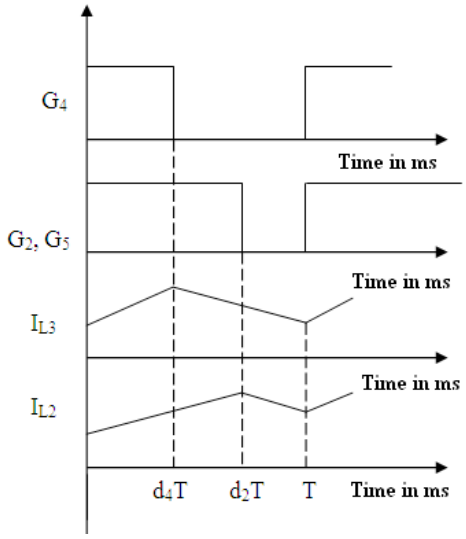

Figure 6. Key waveforms for mode-2 operation.

$P_{wind} = 0$ Where PBAT = power stored in the battery.

$$L_2\frac{di_{L2}}{dt} + r_2 i_{L2} = (d_2 - d_5)V_{PV} + (1-d_2)(V_{PV} - V_0) + d_5(V_{PV} + V_B) \quad (12)$$

$$\frac{L_2\frac{di_{L2}}{dt} + r_2 i_{L2} - V_{PV} - V_B d_5}{(d_2 - 1)} = V_0 \quad (13)$$

$$L_3\frac{di_{L3}}{dt} + r_3\, iL_3 = (d_4 - d_5)V_{FC} + (1-d_4)(V_{FC} - V_0) + d_5(V_{FC} + V_B) \quad (14)$$

$$\frac{L_3\frac{di_{L3}}{dt} + r_3\, iL_3 - V_{FC} - V_B d_5}{(d_4 - 1)} = V_0 \quad (15)$$

$$C_1\frac{dV_0}{dt}+\frac{V_0}{R_0}=i_{L3}+i_{L2}-d_5i_{L3}-d_2i_{L2} \quad (16)$$

3.3 Mode-3 Operation

In mode-3 where PV is poor, the load receives power from wind and FC. The switches S1, S4 and S5 are turned ON and charge the inductors L1 and L3. The current flows through the diodes D1 and D3 by discharging the energy stored in inductors L1 and L3. Figure 7 shows the circuit for this mode of operation and the key waveforms of gate signal and inductor current are shown in Figure 8. The inductor L1 is charged till the switch S1 is turned OFF and it discharges the voltage Vw-V0 into load. Similarly, the inductor L3 is charged until turning off the switch S4 and S5 and it is discharges the voltage VFC-V0 into load. Small signal modeling of the mode-3 operation is derived as follows:

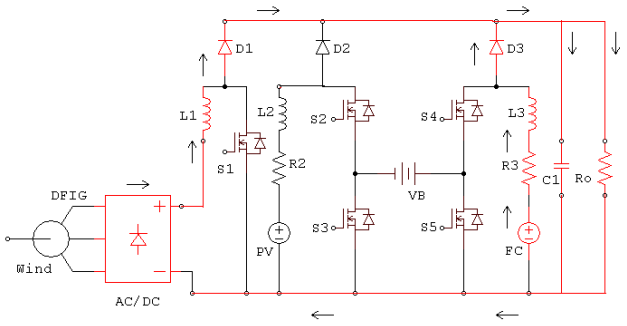

Figure 7. Circuit for operating mode-3.

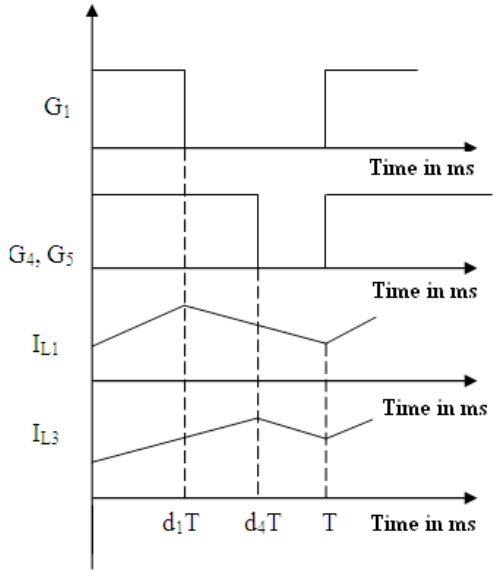

Figure 8. Key waveforms for mode-3 operation.

$$L_1\frac{di_{L1}}{dt}=d_1V_W+(1-d_1)(V_W-V_0) \quad (17)$$

$$\frac{V_W-L_1\frac{di_{L1}}{dt}}{1-d_1}=V_0 \quad (18)$$

$$L_3\frac{di_{L3}}{dt}+r_3i_{L3}=d_4V_{FC}+(1-d_4)(V_{FC}-V_0) \quad (19)$$

$$\frac{V_{FC}-L_3\frac{di_{L3}}{dt}-r_3i_{L3}}{1-d_4}=V_0 \quad (20)$$

$$C_1\frac{dV_0}{dt}+\frac{V_0}{R_0}=i_{L1}(1-d_1)+i_{L3}(1-d_4) \quad (21)$$

3.4 Mode-4 operation

The peak load demand is met in mode-4 by all the input sources. When the switches S1, S2, S3 and S4 are turned ON, the inductors L1, L2 and L3 are charged. At first, the switch S1 is turned OFF to keep the duty ratio D1 less than that of the others. Later, the switch S2 is turned OFF to enable the battery to move into charging mode with extra power. Finally, the switches S4 and S3 are turned OFF and the current flows through the diodes D1, D2 and D3 by discharging the energy stored in inductors L1, L2 and L3. Figure 9 shows the circuit for this mode of operation and the key waveforms of gate signal and inductor current are shown in Figure 10.

The inductors L1, L2 and L3 are charged with voltages VW, VPV, VFC respectively. At first L1 is discharged with voltage VW-V0. Small signal modeling of the mode-4 operation is derived as follows and the energy stored in inductor L1 is similar to mode-1.

$$P_{load}=P_{FC}+P_{wind}+P_{PV} \quad (22)$$

Where *P*FC = power generated by FC.

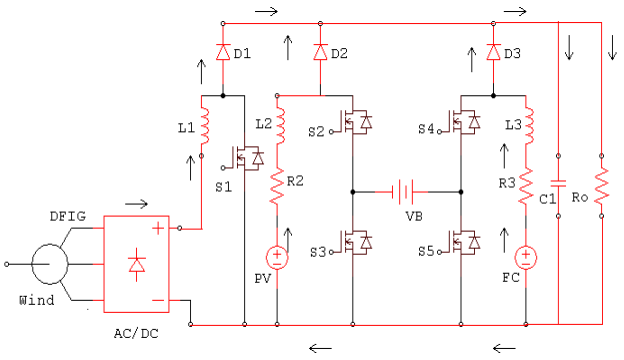

Figure 9. Circuit for operating mode-4.

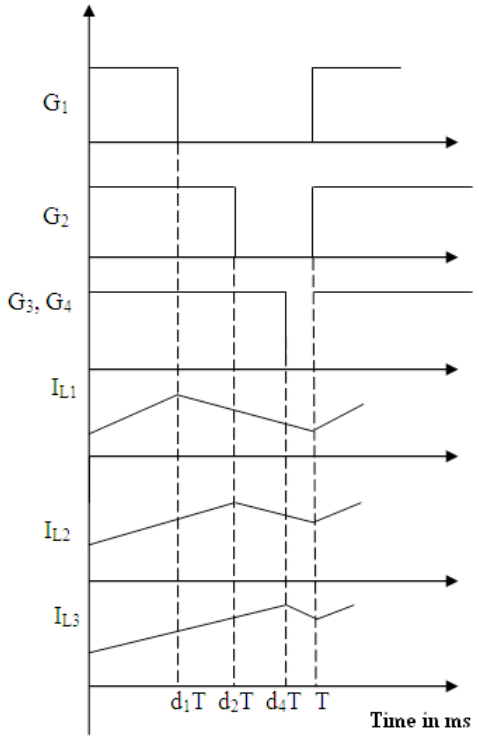

Figure 10. Key waveforms for mode 4 operation.

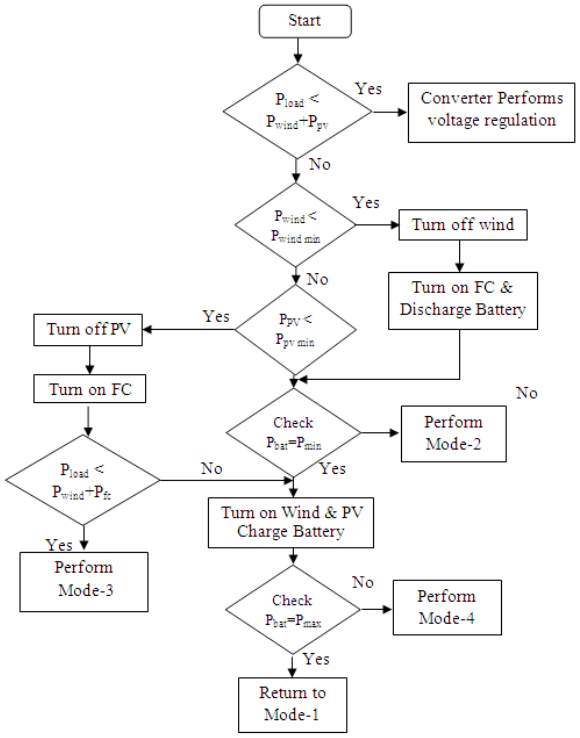

Figure 11. Flow chart for power management.

$$L_1\frac{di_{L1}}{dt} = d_1V_W + (1-d_1)(V_W - V_0) \quad (23)$$

$$\frac{V_W - L_1\frac{di_{L1}}{dt}}{1-d_1} = V_0 \quad (24)$$

$$L_2\frac{di_{L2}}{dt} + r_2i_{L2} = d_3V_{PV} + (1-d_2)(V_{PV} - V_0) + (d_2 - d_3)(V_{PV} - V_B) \quad (25)$$

$$\frac{L_2\frac{di_{L2}}{dt} + r_2i_{L2} - V_{PV} - V_B(d_3 - d_2)}{(d_2 - 1)} = V_0 \quad (26)$$

$$L_3\frac{di_{L3}}{dt} + r_3i_{L3} = d_3V_{FC} + (1-d_4)(V_{FC} - V_0) + (d_4 - d_3)(V_{FC} - V_B) \quad (27)$$

$$\frac{L_3\frac{di_{L3}}{dt} + r_3i_{L3} - V_{FC} - V_B(d_3 - d_4)}{(d_4 - 1)} = V_0 \quad (28)$$

$$C_1\frac{dV_0}{dt} + \frac{V_0}{R_0} = i_{L1}(1-d_1) + i_{L2}(1-d_2) + i_{L3}(1-d_3) \quad (29)$$

3.5 Power Management among the Sources

The power management among the renewable energy sources is shown in Figure11. Consider the initial load demand of 0.75 kW. At first the simulation mode the wind energy and PV meets the load demand of 0.75 kW. If the availability of wind is very less and load demand is not met by this combination, then the wind energy source is shut down fully. In the second simulation mode, FC is turned on and discharging of battery is initiated. If the availability of sunlight is very less and load demand is not met by this combination, then the solar energy source is shut down fully. In the third simulation mode, FC is turned on. In the fourth simulation mode to meet the maximum load demand up to 1.5 kW, the power generation is done by wind, PV and FC and the extra power generated by these sources are utilized to charge the battery. As per the instructions given in the lead acid battery handbook, both charging and discharging are done within the minimum and maximum battery power[23–26]. An 8-s simulation with four dissimilar operating stages is presented to estimate the performance of the converter in every operation mode. Simulation results for the renewable source powers of all combination of input sources are shown in Figure 12.

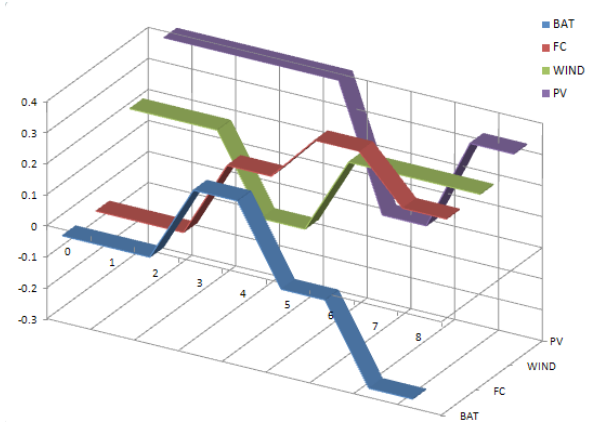

Figure 12. Power sharing of renewable energy sources.

4. Simulation and Experimental Results

Duty ratio for switch 1 is 40%, switch 2 and 3 are supplied with the same duty ratio of 50%. In this mode of operation there is no gate pulse given to switches S4 and S5. The boosted output DC link voltage in all the modes is regulated to vary from 340 V to 350 V. In mode 1 operation the boosted voltage from DC-DC converter is 337.8 V as shown in Figure 13 and the corresponding mode gate pulses are shown in Figure 13. In this mode of operation duty ratio of switch 3 is kept in maximum.

In the laboratory prototype, MOSFET is used as a switching device and its model number IRFPS43N50K is shown in Figure 14. The power diodes model RF2001T3D is used for all the diodes present in the DC-DC boost converter. Power consumed by the controller is not considered during the analysis. The duty ratio of switch S1 should be less than that of S2 and S3. The boosted DC output voltage of 304 V is shown in Figure 15 for mode-1 operation which is slightly less than the simulated voltage. The generation of gate pulses to the switches in the laboratory prototype model is done by a microcontroller. The current passed through the inductor L1 is shown in Figure 16. This figure clearly shows that the L1 is charged till the switch S1 is in ON condition.

5. Modeling and Performance Evaluation

5.1 State Space Modeling

Most of the investigations are done only considering open loop operation. This is due to the multi-port boost convert-

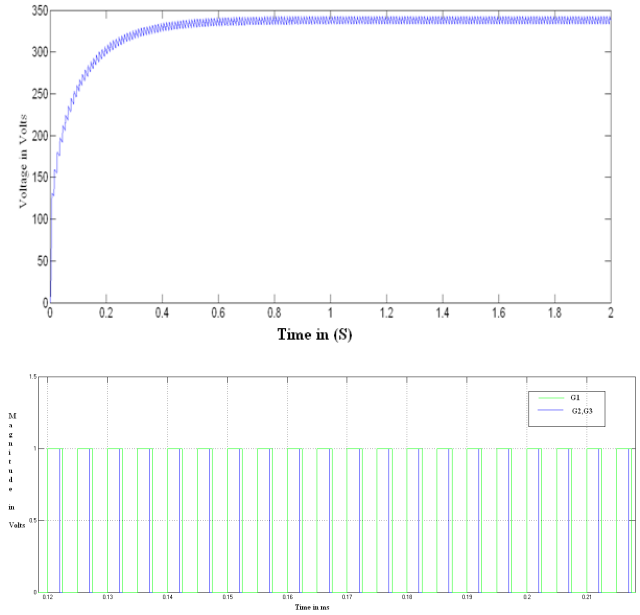

Figure 13. Mode 1 DC link voltage mode 1 gate pulses G1, G2, G3.

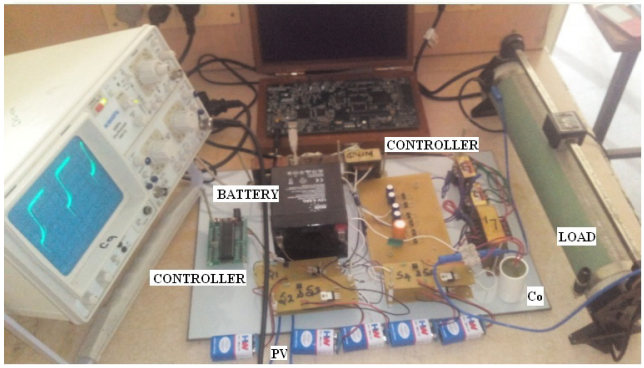

Figure 14. Laboratory prototype model.

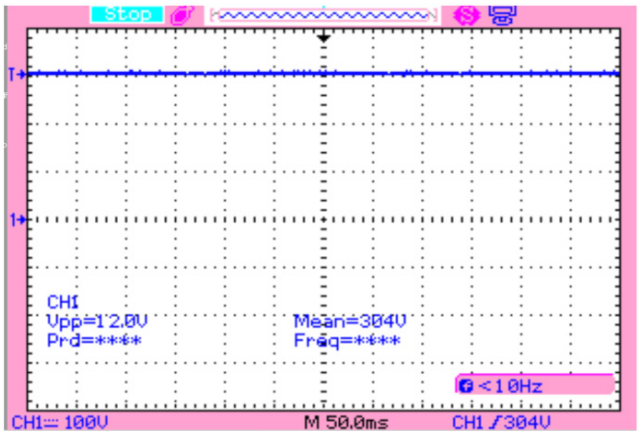

Figure 15. Boosted DC output voltage.

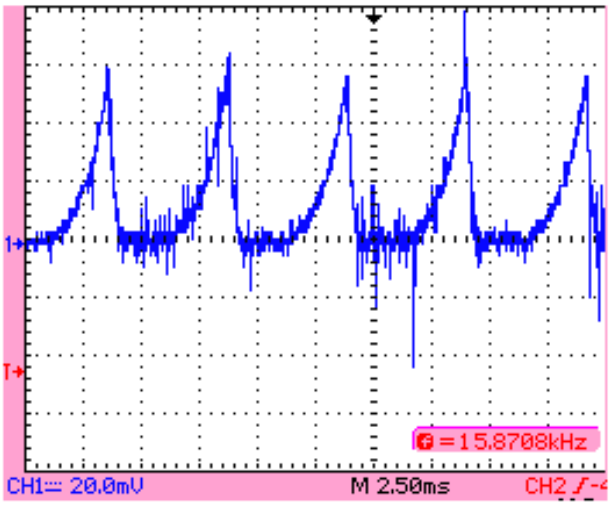

Figure 16. Inductor L1 current for mode 1.

ers are Multiple Input-Multiple Output (MIMO) system that includes many interrelated variables. The dynamic model become much difficult, also the transfer functions are matrix. Interactions among the control variables add considerable difficulty to the design of control system. So, the design of MIMO control system is much difficult than the SISO control system. In this converter, control variables of input differ with mode to mode. To reduce the difficulties associated with controller design of this converter, Multi Input - Multi Output controller design is obtained by deducing the small signal equations and state space modeling. Controllers are properly designed and stable operation of this converter is demonstrated. The average state space modeling is obtained by taking the duty ratios d1, d2, d3, d4 and d5 as control variables. During the mode-1 operation iL1, iL2 and V0 are considered as state variables to derive the state space model.

The state variables are denoted as X, duty ratio is indicated as D and Input voltages are indicated as V. The corresponding perturbations are indicated as x, d, v. These perturbations are very small compared with original values.

$$X' = X+x \tag{30}$$

$$D' = D+d \tag{31}$$

$$V' = V+v \tag{32}$$

Then the small signal equations obtained from mode 1 operation are written in matrix form as follows:

$$\frac{di_{L1}}{dt} = v_w + \frac{(d]_1 - [1)V_0}{L_1} \tag{33}$$

$$\frac{di_{L2}}{dt} = \frac{V_{PV}}{L_2} + \frac{(d]_2 - [1)V_0}{L_2} - \frac{r_2 i_{L2}}{L_2} \tag{34}$$

$$\frac{dv_o}{dt} = \frac{i_{L1}(1-d_1)}{C_1} + \frac{i_{L2}(1-d_2)}{C_1} - \frac{V_0}{C_1 R_0} \tag{35}$$

$$A = \begin{bmatrix} 0 & 0 & \frac{d_1-1}{L_1} \\ 0 & -\frac{r_2}{L_2} & \frac{d_2-1}{L_2} \\ \frac{1-d_1}{C_1} & \frac{1-d_2}{C_1} & -\frac{1}{R_0 C_1} \end{bmatrix} \tag{36}$$

$$B = \begin{bmatrix} \frac{V_0}{L_1} & 0 \\ 0 & \frac{V_0}{L_2} \\ -\frac{I_{L1}}{C_1} & -\frac{I_{L2}}{C_1} \end{bmatrix} \tag{37}$$

$$C = \begin{bmatrix} 1 & 0 & 0 \\ 0 & 1 & 0 \\ 0 & 0 & 0 \end{bmatrix} \tag{38}$$

$$C = \begin{bmatrix} 1 & 0 & 0 \\ 0 & 1 & 0 \\ 0 & 0 & 1 \end{bmatrix} D = [0] \tag{39}$$

Similarly for the mode-2 and mode-3 operations the state space modeling, transfer function model and closed loop control system design are obtained from the following equations:

$$A = \begin{bmatrix} -\frac{r_2}{L_2} & 0 & \frac{d_2-1}{L_2} \\ 0 & -\frac{r_3}{L_3} & \frac{d_4-1}{L_3} \\ \frac{1-d_2}{C_1} & \frac{1-d_4}{C_1} & -\frac{1}{R_0 C_1} \end{bmatrix} \tag{40}$$

$$B = \begin{bmatrix} \frac{V_0}{L_2} & 0 & \frac{V_B}{L_2} \\ 0 & \frac{V_0}{L_3} & \frac{V_B}{L_3} \\ -\frac{I_{L2}}{C_1} & -\frac{I_{L3}}{C_1} & 0 \end{bmatrix} \tag{41}$$

$$C = \begin{bmatrix} 1 & 0 & 0 \\ 0 & 1 & 0 \\ 0 & 0 & 1 \end{bmatrix} \quad (42)$$

Matrix D is feed forward matrix and it is equal to zero.

$$C = \begin{bmatrix} 1 & 0 & 0 \\ 0 & 1 & 0 \\ 0 & 0 & 1 \end{bmatrix} D = [0] \quad (43)$$

In mode-3 operation, only the inductor L1 and Inductor L3 engaged and the equations are given below:

$$A = \begin{bmatrix} 0 & 0 & \frac{d_1 - 1}{L_1} \\ 0 & -\frac{r_3}{L_3} & \frac{d_4 - 1}{L_3} \\ \frac{1 - d_1}{C_1} & \frac{1 - d_4}{C_1} & -\frac{1}{R_0 C_1} \end{bmatrix} \quad (44)$$

$$B = \begin{bmatrix} \frac{V_0}{L_1} & 0 \\ 0 & \frac{V_0}{L_3} \\ -\frac{I_{L2}}{C_1} & -\frac{I_{L3}}{C_1} \end{bmatrix} \quad (45)$$

$$C = \begin{bmatrix} 1 & 0 & 0 \\ 0 & 1 & 0 \\ 0 & 0 & 1 \end{bmatrix} \quad (46)$$

$$D = [0] \quad (47)$$

The absence of iL2 indicates that irradiance is poor during mode-3 operation. The d1 and d4 duty cycle are control variables which is used to regulate the boosted output voltage. In mode-4 operation iL1, iL2 and iL3 and V0 are taken as variables to get matrix "A" and duty ratios d1, d2 and d4 are considered as control variables of the converter.

$$A = \begin{bmatrix} 0 & 0 & 0 & \frac{d_1 - 1}{L_1} \\ 0 & -\frac{r_2}{L_2} & 0 & \frac{d_2 - 1}{L_3} \\ 0 & 0 & -\frac{r_3}{L_3} & \frac{d_4 - 1}{L_3} \\ \frac{1 - d_1}{C_1} & \frac{1 - d_2}{C_1} & \frac{1 - d_4}{C_1} & -\frac{1}{R_0 C_1} \end{bmatrix} \quad (48)$$

$$B = \begin{bmatrix} \frac{V_0 - V_B}{L_2} & 0 & \frac{V_B}{L_2} \\ 0 & \frac{V_0 - V_B}{L_3} & \frac{V_B}{L_3} \\ -\frac{I_{L1}}{C_1} & -\frac{I_{L2}}{C_1} & 0 \end{bmatrix} \quad (49)$$

$$C = \begin{bmatrix} 1 & 0 & 0 & 0 \\ 0 & 1 & 0 & 0 \\ 0 & 0 & 1 & 0 \\ 0 & 0 & 0 & 1 \end{bmatrix} \quad (50)$$

$$D = [0] \quad (51)$$

Feeding the Table 1 values into this matrix A and B, the state space model is obtained by the MATLAB coding. This program generates the equivalent transfer function model and corresponding bode diagram is generated for MIMO as shown in Figure 17. Bode

Table 1. Converter parameters for simulation

Parameter	Values
L1	3 mH
L2	3 mH
C1	200 μF
V0	350 V
D1	40%
D2	50%
r2 , r3	0.2 Ω
R0	250 Ω

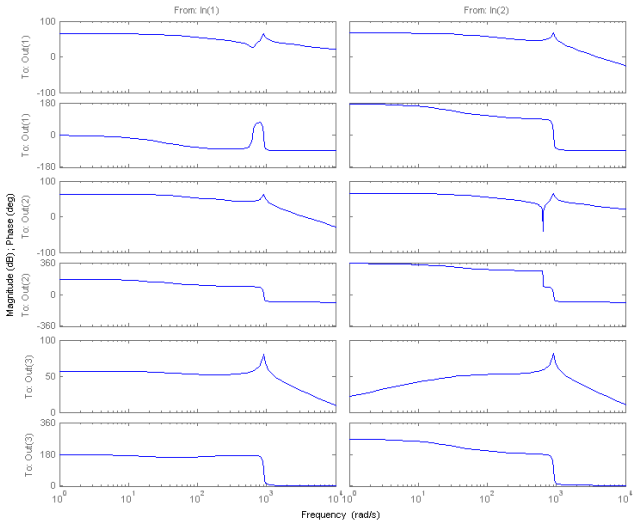

Figure 17. Bode diagram-MIMO.

plot is used to formulate the system compensators. These compensators offer preferred steady state error, satisfactory phase margin, good stability and bandwidth. The bandwidth of the converter during mode-1 is shown in Figure17 (From in 1 to out 1), limitation on this bandwidth leads to decrease the speed of the system responses. Similarly the phase margin shown in Figure 17 (From in 1 to out 1) is not optimum which leads to the system instability. Therefore, utilization of lead compensator is suitable for increasing the cutoff frequency and desired phase margin. The cutoff frequency shown in Figure 17 should be higher after compensation; the bandwidth limitation is also useful to decrease the interaction between control loops. Also low gain at high frequency increases the strength of the system and minimizes the noise. Stable operation of this converter is obtained in all the operating points using properly designed closed loop control system. For loop gain of K = 0.817, the phase margin of 60 degree and gain margin of 10 db are obtained.

5.2 Performance Evaluation

In this proposed multi-port DC-DC boost converter for hybrid power conversion the efficiency improvement of 1% is achieved which is more than the interleaved boost converter. The voltage stress on the power MOSFET switches is calculated for different duty ratios. Compared to conventional in this proposed converter voltage stress is reduced. Comparison of harmonic distortion present in cascaded H-bridge inverter fed interleaved converter and Space Vector Modulation (SVM) inverter fed proposed converter shows the improvement in the quality of multi-port DC-DC converter output voltage.

5.2.1 Comparative Analysis on Converter Efficiency

In this proposed multi-port DC-DC converter the efficiency of the converter topology is checked in terms of power. During the mode-3 operation the maximum power generated is 1.5 kW. Comparative analysis of the efficiency of the proposed converter, efficiency of the interleaved converter and efficiency of the conventional converter are performed. Graphical representation of this comparison is shown in Figure 18 which proves that the proposed converter efficiency is 1% more than the conventional type converters and slightly higher than the interleaved boost converter.

5.2.2 Comparative Analysis on Voltage Stress

In the proposed multi-port converter, L1, L2 and L3 are three inductors of 3 mH connected in series with the input sources. It reduces the voltage stress on the power MOSFET switches considerably and improves the lifecycle of the switches. Lifecycle improvement of the switches is shown in Figure 19. The voltage stress on the switches are calculated in terms of output voltage 1V = V0 of the converter. These inductors are used to reduce the input side current ripples considerably.

The current THD for the proposed system was calculated for five cycles. The FFT analysis is conducted during the simulation. It was found that the THD is 3.85% for the proposed converter with fundamental frequency of 50 Hz. In comparison with the THD of conventional system, the THD obtained from the proposed system was less as shown in Figure 20. In this experiment, the THD was calculated up to 1000 Hz for capturing the fundamental frequency spectrum. The harmonic analysis is conducted in the experimental setup shown in Figure 21. Discussion proves that the performance of the proposed converter is the best suitable converter for hybrid power conversion in all the aspects with a simple compromise on the complex controller design structure.

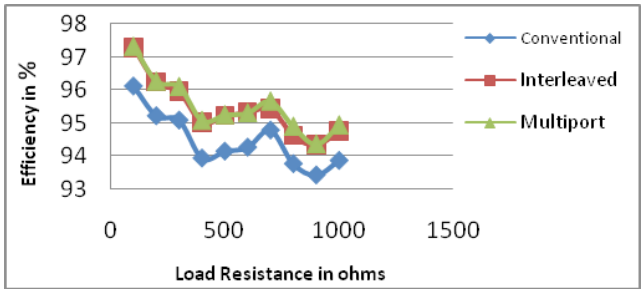

Figure 18. Efficiency improvements in proposed converter.

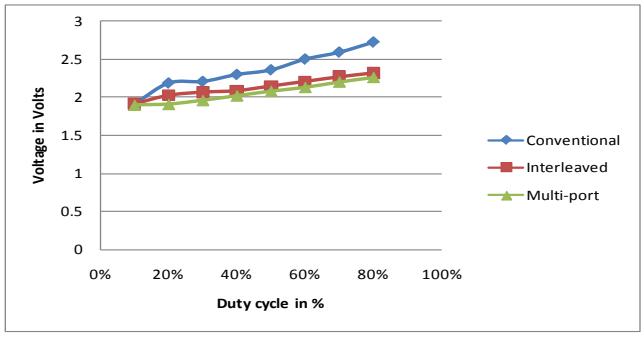

Figure 19. Voltage stress in switching devices.

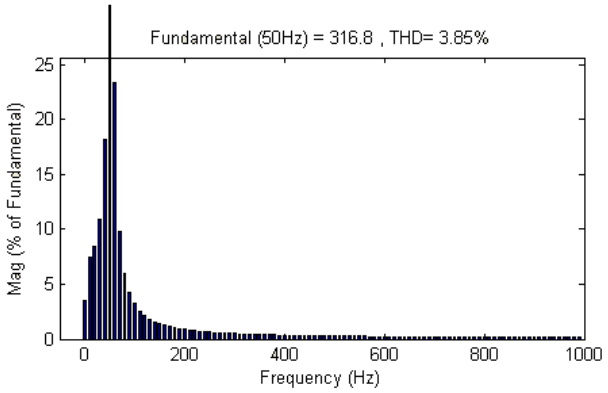

Figure 20. THD on output voltage of inverter fed proposed converter.

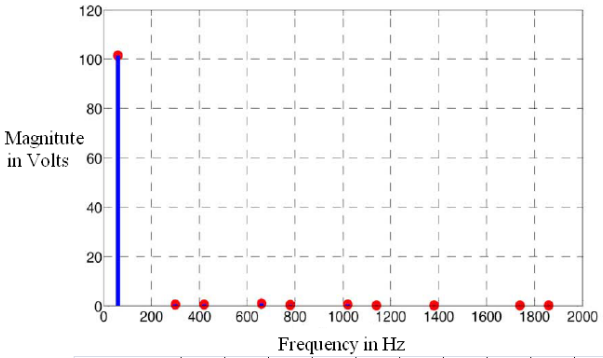

Odd Harmonics	1	3	5	7	9	11	13	15	17	19
% of Harmonics	100	1.44	0.67	0.44	0.33	0.27	0.22	0.19	0.17	0.15

Figure 21. Harmonic spectrum of inverter fed proposed converter.

6. Conclusions

The proposed multi-port converter connects various renewable sources to send energy simultaneously to the load. In the proposed system, primary power sources of energy arise from wind and PV, whereas the FC was used as back up and battery as a long-term storage unit. In this research, a detailed study of the working principle is presented. The steady state equations are obtained to give an insight on component collection and design of hardware. The converter switching losses are reduced by soft switching technique and by utilizing minimum number of switches. The small signal modeling and state space modeling is analyzed for stable operation of the converter. The multi-port DC-DC soft switching boost converter for hybrid power conversion the efficiency improvement of 1% is achieved. In this proposed converter, voltage stress on the switch is less than that of interleaved converter and conventional converter. Further the quality of output voltage is improved with THD of only 3.85% in SVM inverter fed proposed converter which is less than the conventional inverter fed boost converter. Results are presented to show the improved efficiency, fewer harmonic and less voltage stress in the proposed converter.

7. References

1. Tao H, Duarte JL, Hendrix M. Multiport converters for hybrid power sources. IEEE Power Electronics Specialist's Conference; Netherland. 2008. p. 3412–8.
2. Jiang W, Fahimi B. Multiport power electronic interface-concept, modelling and design. IEEE Transactions on Power Electronics. 2011; 26(7):1890–900.
3. Kwasinski A. Quantitative evaluation of DC micro grids availability: Effects of system architecture and converter topology design choices. IEEE Transactions on Power Electronics. 2011; 26(3):835–51.
4. Xu H, Kong L, Wen X. Fuel Cell power system and high power DC-DC converter. IEEE Trans Power Electron. 2004; 19(5):1250–5.
5. Peng F, Li H, Su G, Lawler J. A new ZVS bidirectional DC-DC converter for Fuel Cell and battery application. IEEE Transactions on Power Electronics. 2004; 19(1):54–65.
6. Wu H, Xu P, Hu H, Zhou Z, Xing Y. Full-bridge and bidirectional DC–DC topologies for renewable generation systems. IEEE Trans on Indus Elect. 2014; 61(2):856–69.
7. Kumaran MM, Lakshmi RK. High efficiency DC-DC converter with two input power sources using fuzzy logic controller. IJAIST. 2013; 12(12):1862–75.
8. Choi WY, Lee CG. Photovoltaic panel integrated power conditioning system using a high efficiency step-up DC–DC converter. Renewable Energy. 2012; 41:227–34.
9. Zhang J, Lai JS, Kim RY, Yu W. High-power density design of a soft-switching high-power bidirectional DC–DC converter. IEEE Trans Power Electron. 2007; 22(4):1145–53.
10. Nejabatkhah F, Danyali S, Hosseini SH, Sabahi M, Niapour SM. Modelling and control of a new three-input DC–DC boost converter for hybrid PV/FC/Battery power system. IEEE Transactions on Power Electronics. 2012; 27(5):2309–24.
11. Ravichandrudu K, Madhavi R, Babu YP. Modeling of a novel three-input DC–DC boost converter for PV/FC/battery based hybrid power system. IJEEER. 2013; 3(3):213–28.
12. Hosseini SH, Danyali S, Nejabatkhah FSAK, Niapour M. Multi-input DC boost converter for grid connected hybrid PV/FC/battery power system. Proc IEEE Elect Power Energy Conf; Iran. 2013. p. 1–6.
13. Tao H, Kotsopoulos A, Duarte JL, Hendrix MAM. Multi-input bidirectional DC-DC converter combining DC-link

and magnetic-coupling for Fuel Cell systems. IEEE Industrial Applications Conference. Netherland. 2005; 3:2021–8.
14. Al-Atrash H, Pepper M, Batarseh I. A zero-voltage switching three-port isolated full-bridge converter. IEEE Conference on Telecommunications Energy; USA. 2006. p. 1–8.
15. Al-Atrash H, Batarseh I. Boost-integrated phase-shift full-bridge converter for three-port interface. IEEE Conference on Power Electronics; 2007. p. 2313–21.
16. Zhang Z, Thomsen OC, Andersen MAE, Nielsen HR. A novel dual-input isolated current-fed DC-DC converter for renewable energy system. IEEE Power Electronics Conference and Exposition (APEC); Denmark. 2011. p. 1494–501.
17. Abdel-Rahman O, Batarseh I. An integrated four-port DC-DC converter for renewable energy applications. IEEE Trans Power Electron. 2010; 25(7):1877–87.
18. Husna AWN, Siraj S, Muin MZAB. Modeling of DC-DC converter for solar energy system applications. IEEE Symposium on Computers and Informatics (ISCI); Malaysia. 2012. p. 125–9.
19. Hosseini SH, Danyali S, Gharehpetian GB. New extendable single-stage multi-input DC–DC/AC Boost Converter. IEEE Trans Power Electron. 2014; 29(2):775–88.
20. Hongfei W, Peng X, Haibing H, Zihu Z, Xing Y. Multiport converters based on integration of full-bridge and bidirectional DC–DC topologies for renewable generation systems. IEEE Trans on Indus Elect. 2014; 61(2):856–69.
21. Kuo-Ching T, Chi-Chih H. High step-up high-efficiency interleaved converter with voltage multiplier module for renewable energy system. IEEE Trans on Indus Elect. 2014; 61(3):1311–9.
22. Veena P, Indragandhi V, Jayabharath R, Subramaniyaswamy V. Review of grid integration schemes for renewable power generation system. Renewable and Sustainable Energy Reviews. 2014; 34:628–41.
23. Rani BI, Ilango GS, Nagamani C. Control strategy for power flow management in a PV system supplying DC loads. IEEE Trans on Indus Elect. 2013; 60(8):3185–94.
24. Zeng J, Qiao W, Qu L, Ping Y. An isolated multiport DC-DC converter for simultaneous power management of multiple different renewable energy sources. IEEE Journal of Emerging and Selected Topics in Power Elec. 2014; 2(1):70–8.
25. Santhoshi BK, Sundaram KM, Sivasubramanian M, Akila S. A novel multiport bidirectional dual active bridge DC-DC converter for renewable power generation systems. Indian Journal of Science and Technology. 2016 Jan; 9(1):1–4.
26. Naidu KJ, Harish M, Kittur K. On chip DC-DC converter with high switching frequency and low ripple voltage. Indian Journal of Science and Technology. 2016 Feb; 9(5):1–4.